ANALYSIS AND IDENTIFICATION OF THE APPEARANCE OF UNSTEADINESS EFFECTS IN AN AXIAL COMPRESSOR CASCADE

Ahmadou Bamba DRAME
Departement de génie mécanique
École de Technologie Supérieure
Montréal, Canada
ahmadou-bamba.drame.1@ens.etsmtl.ca

Marlène SANJOSE
Departement de génie mécanique
École de Technologie Supérieure
Montréal, Canada
marlene.sanjose@etsmtl.ca

ABSTRACT

The flow in a rectilinear compressor cascade with a tip gap of less than 2% of chord is investigated using the Shear Blended Eddy Simulation (SBES) hybrid model. In particular the paper focuses on the low-flow rate operating conditions where unsteady flow features near the tip region occur. The Reynolds number is fixed at 4.4×10^5 while the operating condition is controlled by changing the inlet flow angle. The SBES approach allows resolving the turbulent structures of the tip gap flow while efficiently capturing the blade loading with the wall blended Reynolds-Averaged Navier-Stokes modeling. The results show the drastic change of the tip gap flow at the three selected operating conditions. The tip leakage flow analysis shows the vortex breakdown and the vortex disappearance phenomena that contribute to the unsteadiness and the blockage effects close to the clearance region. At near stall conditions, the tip leakage vortex experiences wandering. The flow along the pressure side of the blade a convective modal structures. At partial stall (PS), the tip leakage vortex core disappears, and the modal structure, in the passage along the pressure side, increases in intensity, excited by fluctuations at the leading edge of the blade.

INTRODUCTION

The clearance between the blade tip and the casing wall in a rotating machine is necessary for its proper operation. However, its existence yields complex flow phenomena in the tip region of the gap. This area of unfavorable flow, referred as the tip gap flow is caused by the leakage through the blade and casing wall which is favored by the pressure difference between the pressure and suction sides of the blade. At the clearance exit, the leakage rolls up to form the Tip Leakage Vortex (TLV). The latter interacts with and diffuses into the primary flow and can eventually merge with the blade wake (Lamidel *et al.*, 2021). The tip gap flow is a major source of performance deterioration for axial turbomachinery (Dixon & Hall, 2014). The tip gap flow strengthens and becomes more and more unstable when the flow rate across an axial compressor is decreased. The relationship between the tip gap flow instabilities such as its spiral oscillations and breakdown and the occurrence of partial stall or rotating instabilities issued from spike-inception has been long discussed in the literature (Kameier & Neise, 1997; Vo, 2010; Furukawa *et al.*, 2014; Yamada *et al.*, 2017; Hewkin-Smith *et al.*, 2019). Most of the studies involve experimental measurements or unsteady simulation based on Reynolds Averaged Navier-Stokes simulations.

With the increase in available computational resources for research and the development of advanced scale-resolving approaches, the analysis of turbulence and modal properties of the tip gap flow in isolated airfoil, cascade or low-pressure compressor have recently gained interest (Su *et al.*, 2019). Continuing the investigation of the tip gap flow initiated by Koch *et al.* (2021) of the Virginia Tech compressor cascade at design using Large Eddy Simulation, the present work will present scale-resolved simulations on the same cascade but at several flow-rates, from the best efficiency operating point (BEP) to partial stall (PS). The purpose of this study which will present Shear Blended Eddy Simulations (SBES) at three flow conditions is to identify the progressive change in tip gap flow structure as the incident flow angle is changed. In particular, the unsteadiness of the TLV, its propagation and its influence on turbulent flow properties are investigated.

CONFIGURATION

The investigated rectilinear cascade geometry includes a single blade passage from the 7 passages that compose the experimental section of the Cascade Wind Tunnel operated at Virginia Tech (Muthanna, 1998). The tip leakage flow in this configuration was widely characterized in several experimental campaigns at the BEP (Muthanna & Devenport, 2004; Wenger *et al.*, 2004). The total tunnel height is $H = 254$ mm which also corresponds to the chord $C = 254$ mm of the extruded blade. In the present work, the tip gap height $h = 4$ mm corresponds to 1.6% of the chord. The computational domain is shown in Fig 1. Its dimensions are $4C \times 1C \times 1.5C$ in the streamwise (X), spanwise (Y) and the transverse (Z) directions respectively. The lower wall mimics the casing wall in a turbomachine. It is located at the coordinate $Y = 0$ facing the tip of the blade.

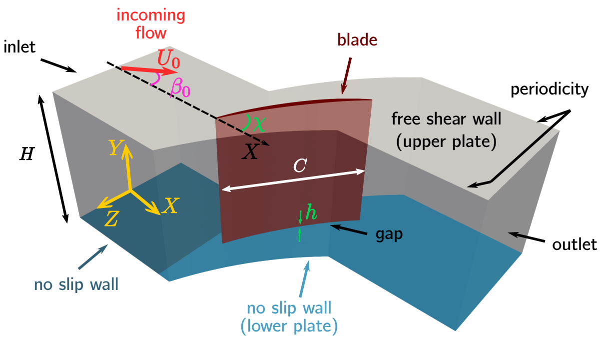

Figure 1. Numerical domain used for the computations.

The boundary conditions are identified in Fig 1. Periodic conditions are applied in the transverse direction, whereas no-slip conditions are specified everywhere except on the upper wall where no shear is applied to simplify the resolution. The upstream velocity U_0 corresponds to the relative velocity of the flow as seen by the blade. The angle β_0 corresponds to the angle of the flow with respect to the machine direction (X). The flow angle $\phi = 1/\tan\beta_0$ is defined from the incoming velocity components.

In the present work, the velocity intensity is kept at $U_0 = 25.2$ m/s. Three simulations are performed for β_0 equal to $65.1°$, $69.1°$ and $72.1°$ i.e. for ϕ equal to 0.464, 0.382 and 0.323 respectively. These operating points were carefully selected to represent the Best Efficiency Point (BEP), Near Stall (NS), and Partial Stall (PS) respectively. The Reynolds number based on the blade chord is therefore identical in the three simulations at $Re_c = 4.4 \times 10^5$. The Mach number is $Ma = 0.07$, which justifies the incompressible approach adopted in the simulations. The air density is set to $\rho = 1.185$ kg/m^3.

The Shear Blended Eddy simulations (SBES) are performed with the ANSYS CFX solver 2021.R2. The idea behind SBES is very straightforward: RANS and LES models are combined to compute the viscous stress tensor through a blending function which activates the RANS portion of the model not for the entire boundary layer, but only for the region very close to the wall. In other regions (wake, gap), the turbulence is resolved with LES approach (Menter, 2018).

The initial grid designed in the work of Koch *et al.* (2021) is used for the BEP. It consists of 135×10^6 cells with prismatic layers on the blade surface and on the lower plate, and tetrahedral elsewhere. This mesh is sufficiently refined near the tip gap and in the wake in order to capture the main and the small vortex structures. The wall resolution wall units (y^+) is between $1 < y^+ < 2$ on the suction and pressure sides. For the two lower flow rates, as the flow might massively separate from the walls, the initial grid is slightly modified to capture tip gap flow in the blade passage and upstream of the leading-edge, by extending refinement zones in these areas.

The calculation performed with the High Resolution advection scheme (ANSYS, Inc, 2022). The timestep is fixed at 13 μs to ensure a CFL number lower than one in the entire domain. The L2-norm equation residuals are converged up to 5×10^{-5} within 3 sub-iterations by physical timestep. After flow establishment has been confirmed, the three simulations are run for a total physical time of $10T_c$, where $T_c = C/U_0$ is the through-flow time over the blade chord.

Overall performances

Before evaluating the unsteadiness associated with the tip leakage vortex in this configuration, the aerodynamic performance is first verified. In the context of a incompressible cascade flow, the pressure coefficient ψ is evaluated from the static pressure gain across the cascade, and the efficiency η is obtained from the total pressure losses as given below:

$$\psi = \frac{P_{\text{outlet}} - P_{\text{inlet}}}{\frac{1}{2}\rho U_0^2} \tag{1}$$

$$\eta = 1 - \frac{P_{0,\text{inlet}} - P_{0,\text{outlet}}}{\frac{1}{2}\rho U_0^2} \tag{2}$$

where P_{inlet} and P_{outlet} are mass flow averaged static pressure at inlet and outlet respectively and $P_{0,\text{inlet}}$ and $P_{0,\text{outlet}}$ are mass flow averaged total pressure at inlet and outlet respectively.

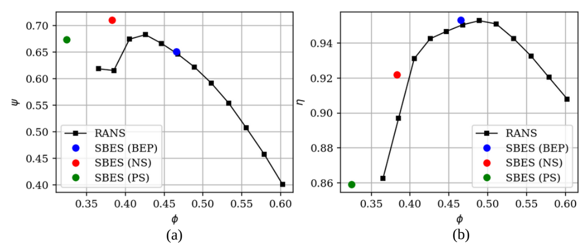

Figure 2. Comparison of RANS and SBES calculation - (a) : Static pressure rise ψ ; (b) : Efficiency η.

Figure 2 compares the efficiency and pressure coefficient obtained from RANS and SBES simulations. RANS calculations were performed on the same configuration using the $k-\omega$ SST turbulent model closure for ϕ values ranging from 0.325 to 0.601 (Drame & Sanjose, 2023). Both RANS and SBES simulations show similar performance at BEP, but significant differences arise at lower flow coefficients due to the emergence of unsteady mechanisms. The maximum pressure rise occurs at $\phi = 0.422$ with the RANS approach, but is delayed to $\phi = 0.381$ with the SBES approach. At this point, identified as near-stall, the efficiency is reduced by 3% compared to BEP. At $\phi = 0.323$, the pressure rise is still significant with the SBES approach, while it has decreased with the RANS approach. However, the efficiency has dropped for both approaches. For this operating condition, the cascade is partially stalled as it still produces a significant pressure rise.

Tip gap flow analysis

Figure 3 shows flow fields in a plane parallel to the lower plate (or casing wall), located 5%H above it. At this location, the flow patterns are strongly influenced by the tip gap flow. The instantaneous velocity magnitude for the three investigated flow coefficients is displayed on the left in Fig 3. At this location, close to the clearance, the flow is highly influenced by the tip gap flow. At BEP and NS, the background velocity decreases at the entrance of the blade passage as pressure builds up in the compressor cascade. Intense velocity amplitudes are observed close to the suction side where the tip vortex is located, superimposed on the main flow. The low

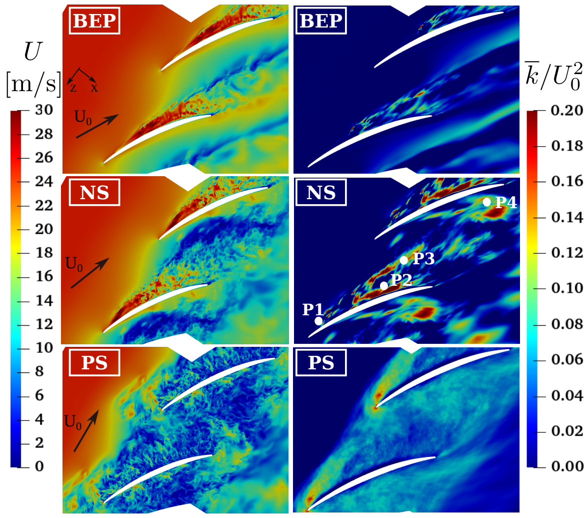

Figure 3. Instantaneous velocity magnitude (left) and time-averaged turbulent intensity (right) in a blade-to-blade plane at 5%H above the lower plate for BEP, NS and PS flow conditions from top to bottom.

velocity amplitudes show the blockage effect caused by the tip vortex. At BEP, a thin zone is visible in the middle of the blade passage after mid-chord. At NS, the area is larger and has reached the pressure side of the adjacent blade. At PS, the velocity decreases already upstream from the leading edge, and the full blade passage is blocked at this span location. Small pockets of mild velocity randomly pass through the blockage, and larger spots of high velocity appear, interacting with the leading and trailing edges.

The unsteadiness of the flow can be determined by the Turbulent Kinetic Energy (k), which is the kinetic energy associated with the velocity fluctuations, resolved in time and space in the SBES simulations. The TKE k is calculated using equation (3), where u, v and w represent the instantaneous velocity components and the overbar indicates the time average.

$$k = \frac{1}{2}\left[(u-\overline{u})^2 + (v-\overline{v})^2 + (w-\overline{w})^2\right] \tag{3}$$

In Figure 3, the right side displays the time-averaged intensity of the resolved TKE $\overline{k}/U_0^2$ in a blade-to-blade plane 5%H away from the casing wall for the three flow coefficients. The turbulent intensity in the blade passage in distributed very differently for the three investigated operating conditions. At BEP, the turbulent intensity is minimal except for intense spots after mid-chord in the vicinity of the blade suction side. At NS, spots are larger and more intense. They appear already after quarter-chord in the vicinity of the blade suction side. An additional large area of turbulent intensity appear in the rear of the passage close to the pressure side of the adjacent blade. At NS, the turbulent intensity is more diffused and covers the full passage. Intense levels appear at the leading edge aligned with the Z direction.

In Fig 4, the resolved vortices in the three SBES simulations are identified by an isosurface of instantaneous Q criterion. As expected with this hybrid approach, the turbulence in the boundary layers is not resolved, but the vortices associated to both the tip gap flow and the wake flow are well resolved. At BEP, the SBES results provide a detailed view of the observation that has been made for a long time (Inoue & Kuroumaru, 1989). The TLV is coherent and clearly visible from the leading-edge of the blade, where it is very thin along the blade edge, to downstream of the blade passage, where it appears as the vortex core of a more complex structure. At about 40% of the chord, the TLV is caught up with the leakage jet flow perpendicular to the blade coming from the pressure side through the clearance (below the edge from the shown point-of-view). Consequently, the TLV moves away from the blade edge and vortex breakdown happens progressively. The merged structure is surrounded by rings of induced vortices (IV) that are fed by the leakage jet flow. In the initial development phase of the TLV, a thin IV is also visible, which impinges on the blade. The spots of turbulent intensity seen in Fig 3 (top right) are related to the intense shear caused by the IV, while the low intensity zone is the locus of the TLV core. At BEP, the resolved turbulent eddies in the wake are limited to vortex shedding (VS) generated at the rounded trailing edge.

At NS, in the center of Fig 4, the same vortical structures can be identified, but with a larger spread and increased complexity. The leakage jet flow exits the clearance earlier, at around 20% of the chord, due to the larger pressure rise at this operating condition, pushing the TLV away from the tip edge much earlier. The strength of the leakage jet flow causes the TLV core to have a wavy shape and results in a more rapid and intense vortex breakdown. The rings of the IV impact the blade at several locations. On their opposite flanks, they propagate parallel to the pressure side of the adjacent blade towards its trailing edge. For this operating condition also, the IV structure can be associated with the high turbulence intensity zones seen in Fig 3 (center right). The wake flow is still marked by the VS, but additional vortices are resolved in the suction side part of the wake, caused by the thickening of the boundary layer.

Turbulent structures are present throughout the passage at PS, and a clear TLV structure cannot be identified in the right of Fig 4. Vortices of larger characteristic sizes, compared to the other two operating conditions, can be observed passing through the passage at higher speeds (red). Several authors Vo (2010); Yamada *et al.* (2017); Pullan *et al.* (2015) have identified the formation of a tornado-like vortex at the leading edge using unsteady RANS approaches, due to the spillage of leakage jet flow towards the adjacent blade. The tornado structure is visible is the SBES snapshot, almost perpendicular to the chord. This is consistent with the expected type of stall for the current tip clearance size of 1.6% chord (Hewkin-Smith *et al.*, 2019). The large turbulent eddies shedded into the blade passage are caused by this tornado-like structure. The massive blockage causes the formation of a horseshoe vortex upstream of the leading-edge. The tip gap flow finally merges with the wake. Close to the upper plate (hub wall), the wake flow remains thin and is still strongly marked by the VS instability.

To further characterize the level of turbulence in the blade passage, a spectral analysis is performed. Probes were strategically positioned in the blade passage to capture all turbulence information for the three flow coefficients. The probe positions are identified by the white dots in Fig 3. Signal is recorded at these locations at every timestep which correspond to a sampling frequency $f_s = 77$ kHz, and the instantaneous axial velocity component is scaled by the inlet velocity U_0. The power spectral density is computed using the Welch's periodogram technique. In the present case, Hanning windows of 870 points and 66% overlap are used yielding a resolution frequency of 88 Hz. The obtained spectra are displayed in Fig 5 for the three flow coefficients.

At all probe locations, the BEP spectra have the smallest turbulence level. The spectra associated with the PS operating

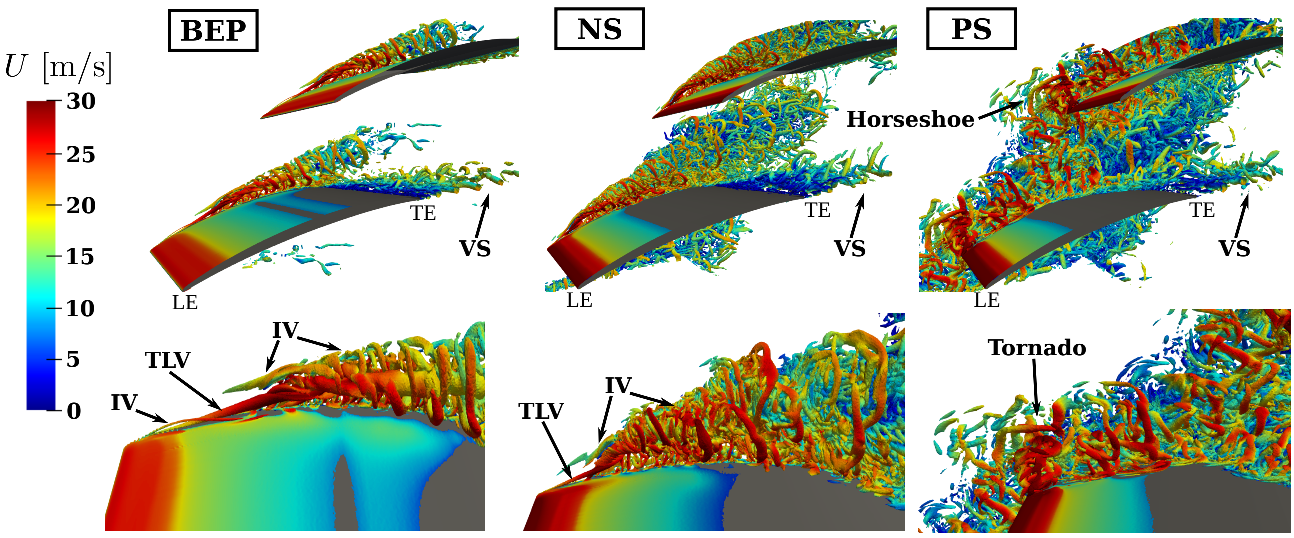

Figure 4. Isosurface of Q criterion with value 10^6 s^{-2} at three flow conditions: BEP (left), NS (center), PS (right). Global isometric view of the blade passage from the upper plate (top); zoom on leading-edge to mid-chord, close to gap (bottom).

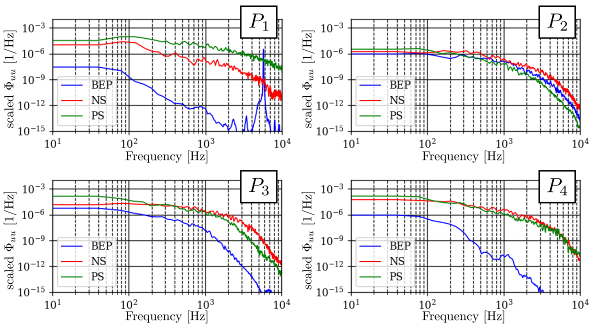

Figure 5. Spectral Density of the axial velocity at 5%H near the gap at probe locations shown in Fig 3.

condition show the highest turbulent levels in the passage entrance (P_1), while the levels of the NS configuration are dominant in the blade passage (P_2, P_3, P_4). These observations are consistent with the previous fields in Figs 3 and 4. At P_1, the BEP shows an intense tone at 6 kHz that is associated with an instability of the IV vortex, which could also be an artifact of the SBES approach. On the opposite, the PS config shows a fully turbulent spectra, with maximum energy at low frequency, that is at large scales. At P_2 close to the suction side, all configurations show similar turbulence levels, while at P_3 in the center of the passage, the levels of NS and PS increase, with the PS configuration showing higher energy at low frequencies. At P_4 close the trailing edge on the pressure side of the adjacent blade, the BEP turbulent energy has dropped while the other two configurations show broad turbulent spectra. The hump at 1 kHz at BEP is characteristic of the VS mechanism identified in the wake and can only be seen for BEP because of the low background turbulence levels in this optimal flow condition.

Wall pressure fluctuations

To characterize the influence of the tip gap flow on the unsteady loading, the standard deviation of the wall pressure is computed. To compare accurately between the different operating conditions, the statistics is given in the form of a pressure coefficient $C_{p'_{\mathrm{rms}}}$. The later is computed using Eq. 4 where

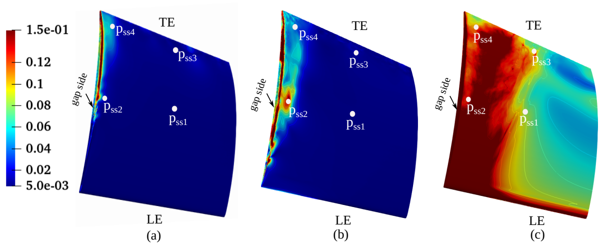

Figure 6. Standard deviation of the pressure coefficient on the blade $C_{p'_{\mathrm{rms}}}$ - (a) : BEP; (b) : NS; (c) : PS.

$p' = p - \overline{p}$ is the local wall pressure fluctuation.

$$C_{p'_{\mathrm{rms}}} = \frac{\sqrt{\overline{p'^2}}}{\frac{1}{2}\rho U_0^2} \quad (4)$$

Figure 6 shows $C_{p'_{\mathrm{rms}}}$ on the blade suction side for the three flow coefficients. As the flow coefficient decreases, the area of the blade affected by the turbulent fluctuations generated by the tip gap flow increases. At BEP, only a narrow portion at the rear of the blade tip (after 40% C) shows significant levels. This is the location where the IV rings scrap on the blade surface. At NS, the high levels appear upstream near the leading edge, and occupy a larger portion of the span still associated with the IV rings scrapping. At PS, high levels are seen all over the blade for almost half of the blade. In addition, high levels are seen at the leading edge over the entire span, indicating an increase in upstream turbulence levels over the entire passage.

A spectral analysis is performed at the four positions on the suction side of the blade (P_{ss1}, P_{ss2}, P_{ss3}, and P_{ss4}) marked with white dots in Fig 6. Identical settings are used in the Welch's periodogram technique as before. Figure 7 shows the wall pressure spectral density (PSD) for the three operating conditions.

At mid-span in Fig 7 (left), at probe locations P_{ss1} and P_{ss3} on the blade suction side, the fluctuation levels in the PS configuration are the dominant ones, showing that the complex tip gap flow at this regime influences 50% of the global blade

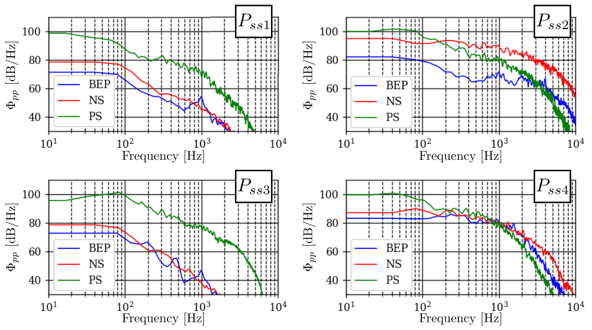

Figure 7. Spectral density of the wall-pressure fluctuations on the suction side at probe locations shown in Fig 6.

passage. At these locations, the BEP and NS configurations show low levels similarly. The VS frequency at 1 kHz identified in Fig 5 is again visible in the BEP spectrum where the turbulent fluctuations are low. Near the tip in Fig 7 at probe location P_{ss2}, the NS spectrum is dominant at high frequencies. The probe P_{ss2} is actually located in an impact location of the IV rings, which wrap around the wandering TLV for this operating condition. The PS spectrum shows the highest levels at low frequencies due to the large turbulent eddies associated with the tornado vortex structure. Near the tip in Fig 7 at trailing edge at probe location P_{ss4}, the three spectra have similar levels around 800 Hz. The PS spectrum shows higher levels at low frequencies and a faster decay at high frequencies, which is typical of turbulence associated with large scale eddies. The NS spectrum has larger levels by about 5 dB/Hz than BEP at low and high frequencies.

Modal analysis

Figure 8 shows instantaneous pressure coefficient C_p defined by Eq. (5) for the three flow coefficients at two distinct random instants in the plane parallel to the casing at 5% H.

$$C_p = \frac{p - P_{\mathrm{outlet}}}{\frac{1}{2}\rho U_0^2} \tag{5}$$

As the flow coefficient decreases, more perturbed flow patterns are visible. The TLV core can be identified by the dark blue line which identify the low pressure vortex center. At BEP, the two snapshots are very similar highlighting that no unsteadiness is occurring in the vortex core. The vortex separates from the blade around 40%C. As previously observed in the literature (Furukawa *et al.*, 2014) the TLV is stable at BEP. At NS configuration, the TLV core separates from the blade further upstream around 10%C and with a trajectory further towards the passage center. The vortex core has different instantaneous positions, strengths and shapes, highlighting natural instability, which is also known as the vortex wandering (Mailach *et al.*, 2000; Furukawa *et al.*, 2014). At PS, the vortex core is not visible. Instantaneous C_p patterns are highly different between the two snapshots. Perturbation and non homogeneity are clearly visible upstream of the leading edge, identifying the spillage of leakage jet flow (Vo, 2010; Hewkin-Smith *et al.*, 2019).

In the same plane and for the same instants as in Fig 8, fluctuations of pressure coefficient $C_{p'}$ given by Eq. (6) are

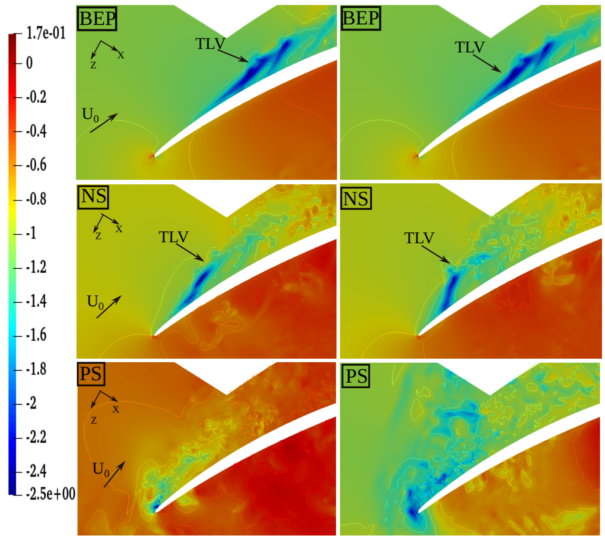

Figure 8. Instantaneous pressure coefficient (C_p) at 5%H near the gap - instant t_1 (left); instant t_2 (right)

shown for the three flow coefficients in Fig 9.

$$C_{p'} = \frac{p'}{\frac{1}{2}\rho U_0^2} \tag{6}$$

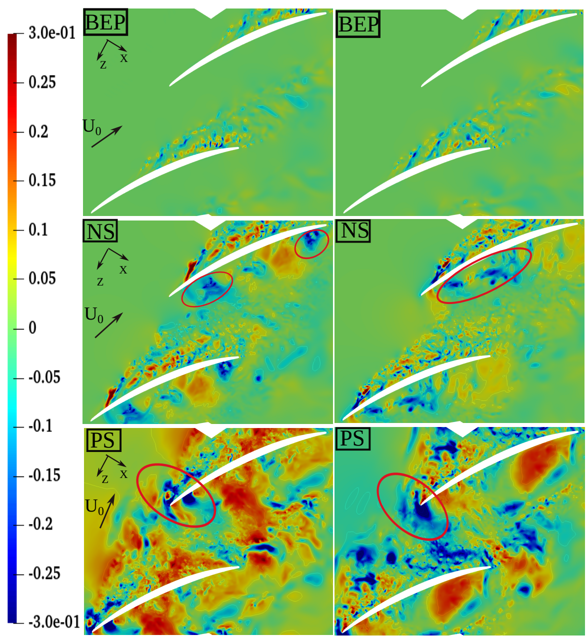

Figure 9. Fluctuating pressure coefficient $C_{p'}$ at 5% H near the gap - instant t_1 (left); instant t_2 (right)

At BEP, pressure fluctuations are only visible in the TLV after 40%C once the coherent core has separated from the blade, as identified in Fig 4 (left) and 8 (top). At NS, fluctuations are similarly visible in the TLV. They appear as more intense spots and already after 10%C from the leading edge. The distinctive feature of this operating condition is the perturbations seen along the pressure side of the neighboring blade. The fluctuations form large coherent positive and negative lobes that propagate in alternance as can be interpreted from the two snapshots. These patterns are probably associated with the large IV rings that occupy the entire blade passage at NS. At PS, fluctuations appear everywhere coherently with the vortices already identified in Fig 4 (right) and the TKE intensity levels covering the full passage in Fig 3 (bottom right). In addition, intense large spots impinging the neighboring blade leading edge are noticeable. The same lobe propagation patterns below the pressure side of the blade are visible as for NS case but with larger characteristic sizes. This explains the higher levels at low frequencies in the spectra in Figs 5 and 7.

Conclusion

Numerical simulations of the compressor cascade of Virginia Tech (VT) using the hybrid Shear-Blended Eddy Simulation (SBES) approach for three different flow coefficients corresponding to the best efficiency point (BEP), the near stall point (NS) at maximum pressure rise and a partial stall point (PS), where 50% of the span is stalled, have been performed. The overall performances between SBES and RANS are identical at BEP, but pressure rise is higher at NS and PS conditions highlighting the role of unsteady flow patterns at these operating conditions. As flow coefficient is reduced, low velocity areas occupy the entire space in the blade passage until stall occurs. The use of a scale-resolved approach like SBES allows identifying the turbulent eddies associated with the tip gap flow. The well documented tip gap flow structure can be observed in this canonical configuration at BEP with great details. Induced Vortex (IV) rings wrap around the Tip Leakage Vortex (TLV) and contribute to its progressive breakdown. The IV rings cause turbulent fluctuations in the blade passage and on the tip of the blade. At NS, the tip gap flow structure extends to the entire blade passage near the tip. The TLV separates further upstream from the blade and the IV rings grow progressively up to the pressure side of the adjacent blade. Their scrapping over the blade surface is still limited to the tip of the blade, but the wall-pressure fluctuations levels are largely increased compared to BEP. At PS, the TLV structure cannot be identified anymore in the complex tip gap flow. A tornado like coherent structure caused by the spillage of the leakage jet flow, can be identified in the SBES snapshots at the leading edge of the blade, almost perpendicular the chord. The tornado like structure is shown to be responsible to the propagation of large turbulent eddies in the blade passage. These unsteady and coherent patterns cause an increase in turbulent levels at low frequencies.

To characterize these unsteady mechanisms at NS and PS conditions, a dynamic modal analysis (DMD) will be performed in a near future to identify and characterize the dominants frequencies that are associated with the stall of the VT compressor cascade.

REFERENCES

ANSYS, Inc 2022 CFX-Solver Theory Guide. Documentation 2022.R2. Canonsburg, PA.

Dixon, S. L. & Hall, C. A. 2014 *Fluid Mechanics and Thermodynamics of Turbomachinery*, seventh edition edn. Amsterdam ; Boston: Butterworth-Heinemann is an imprint of Elsevier.

Drame, A.B & Sanjose, M 2023 Analyse, classification et modélisation des pertes dans une grille rectiligne de compresseur avec jeu. In *Computational Fluid Dynamics Canada International Congress*, p. 6. Sherbrooke, Canada.

Furukawa, M, Saiki, K, Yamada, K & Inoue, M 2014 Unsteady Flow Behavior due to Breakdown of Tip Leakage Vortex in an Axial Compressor Rotor at Near-Stall Condition. In *ASME Turbo Expo 2000: Power for Land, Sea, and Air*. American Society of Mechanical Engineers Digital Collection.

Hewkin-Smith, M., Pullan, G., Grimshaw, S. D., Greitzer, E. M. & Spakovszky, Z. S. 2019 The Role of Tip Leakage Flow in Spike-Type Rotating Stall Inception. *Journal of Turbomachinery* **141** (061010).

Inoue, M. & Kuroumaru, M. 1989 Structure of Tip Clearance Flow in an Isolated Axial Compressor Rotor. *Journal of Turbomachinery* **111** (3), 250–256.

Kameier, F. & Neise, W. 1997 Experimental Study of Tip Clearance Losses and Noise in Axial Turbomachines and Their Reduction. *Journal of Turbomachinery* **119** (3), 460–471.

Koch, R, Sanjosé, M & Moreau, S 2021 Aerodynamic investigation of a linear cascade with tip gap using large-eddy simulation. *Journal of the Global Power and Propulsion Society* **5**, 39–49.

Lamidel, David, Daviller, Guillaume, Roger, Michel & Posson, Hélène 2021 Numerical Prediction of the Aerodynamics and Acoustics of a Tip Leakage Flow Using Large-Eddy Simulation. *International Journal of Turbomachinery, Propulsion and Power* **6** (3), 27.

Mailach, R., Lehmann, I. & Vogeler, K. 2000 Rotating Instabilities in an Axial Compressor Originating From the Fluctuating Blade Tip Vortex. *Journal of Turbomachinery* **123** (3), 453–460.

Menter, F. 2018 Stress-blended eddy simulation (SBES)—A new paradigm in hybrid RANS-LES modeling. In *Progress in Hybrid RANS-LES Modelling* (ed. Yannick Hoarau, Shia-Hui Peng, Dieter Schwamborn & Alistair Revell), pp. 27–37. Cham: Springer International Publishing.

Muthanna, Chittiappa 1998 Flowfield Downstream of a Compressor Cascade with Tip Leakage. PhD thesis, Université de Floride, Virginia Technology.

Muthanna, C & Devenport, William J. 2004 Wake of a Compressor Cascade with Tip Gap, Part 1: Mean Flow and Turbulence Structure. *AIAA Journal* **42** (11), 2320–2331.

Pullan, G., Young, A. M., Day, I. J., Greitzer, E. M. & Spakovszky, Z. S. 2015 Origins and Structure of Spike-Type Rotating Stall. *Journal of Turbomachinery* **137** (051007).

Su, Xiangyu, Ren, Xiaodong, Li, Xuesong & Gu, Chunwei 2019 Unsteadiness of Tip Leakage Flow in the Detached-Eddy Simulation on a Transonic Rotor with Vortex Breakdown Phenomenon. *Energies* **12** (5), 954.

Vo, Huu D. 2010 Role of Tip Clearance Flow in Rotating Instabilities and Nonsynchronous Vibrations. *Journal of Propulsion and Power* **26** (3), 556–561.

Wenger, Christian W., Devenport, William J., Wittmer, Kenneth S. & Muthanna, Chittiappa 2004 Wake of a Compressor Cascade with Tip Gap, Part 3: Two Point Statistics. *AIAA Journal* **42** (11), 2341–2346.

Yamada, Kazutoyo, Furukawa, Masato, Tamura, Yuki, Saito, Seishiro, Matsuoka, Akinori & Nakayama, Kentaro 2017 Large-Scale Detached-Eddy Simulation Analysis of Stall Inception Process in a Multistage Axial Flow Compressor. *Journal of Turbomachinery* **139** (7).